IPSJ Transactions on Mathematical Modeling and Its Applications Vol.9 No.3 24–31 (Dec. 2016)

Regular Paper

Model Selection of Early Vision System of *Drosophila melanogaster*

Hideaki Ikeda[1,a)] Yoshinori Suzuki[2] Takako Morimoto[3] Toru Aonishi[4]

Received: June 4, 2016, Revised: July 25, 2016/August 4, 2016,
Accepted: August 17, 2016

Abstract: Several quantitative models of motion-sensitive neurons called lobula plate tangential cells (LPTCs) in the fly visual system have been proposed: The four-detector (4D), six-detector (6D) models and the two-detector (2D) model. Here, we select the most suitable model from the above three ones by fitting electrophysiological data of LPTCs in responses to motion stimuli. We calculated generalization errors (GEs) of the models by cross-validation method. Due to the result of cross-validation and non-reasonability of the 4D and 6D models fitted to the electrophysiological data, we can select the 2D model.

Keywords: Fly's motion vision, correlation-type model, model selection, neural coding, Lobula plate tangential cell, elementary motion detector, electrophysiological data

1. Introduction

Detecting a direction of image motion is a fundamental element in visual computation and is essential for survival because motion occurs when an animal is moving in its environment [1], [2]. Insect motion vision has been well-known as an effective example for studying fundamental principles of information processing in visual system [2], [3]. The fly's visual system including fruit fly *Drosophila melanogaster* has been received attention as a model organism in systems neuroscience due to the availability of a wide range of genetic tools for manipulating and dissecting neural circuits [2], [3]. Furthermore, the combination of physiological recording and genetic manipulation has been established in *Drosophila melanogaster* [1], [2]. Although the fly's visual system shares similar structural and functional traits with that of vertebrates [4], [5], the fly's nervous system contains only a few hundred thousand neurons as opposed to billions and more in the vertebrate central nervous system [1], [2]. This simplicity makes us possible to analyze circuits in the fly's nervous system more effective, at least to some extent [1], [2].

The visual ganglia in the fly visual system consist of four different layers called the lamina, the medulla, the lobula and the lobula plate [1], [2]. Motion-evoked behaviors in *Drosophila* depend on R1-R6 photoreceptors as well as their immediate postsynaptic targets, the lamina monopolar cells L1 and L2 cells [2], [6]. There are two major separated pathways called the L1 and L2 pathway that L1 and L2 cells relay signals to the medulla respectively [2], [3]. The signals are finally transmitted to the third-order neuropil consisting of lobula and lobula plate [2], [3]. In the lobula plate, large directionally selective tangential cells, which are called lobula plate tangential cells (LPTCs), extend their elaborate dendrites and spatially integrate the output of local presynaptic motion detectors [2], [3]. In the context of neural coding in the fly visual system, it has been remained controversial whether the L1 and L2 pathways could code OFF-ON and ON-OFF sequence stimuli [7], [8], [9].

There are the following three typical models of elementary motion detection (EMD) models that are classified into the correlation-type model [7], [10]. The four-detector (4D) model (**Fig. 1** B), which consists of four standard Reichardt detector units (SRD units) (Fig. 1 A), had been proposed to address the issue on the difficulty of the biological implementation of the SRD unit. Furthermore, the two-detector (2D) model (Fig. 1 D) and six-detector (6D) model (Fig. 1 C), which consist of two and six SRD units respectively, had been proposed under different hypothesis on whether or not the L1 and L2 pathways could respond to ON-OFF and OFF-ON sequence stimuli [3], [6], [7].

In this paper, we sought quantitatively to select the most appropriate model from the three models using the common experimental data set. We used electrophysiological data reported in Suzuki et al. [11], which consists of membrane potential traces of LPTCs in response to panoramic vertically striped square-wave grating rotating in both preferred direction (PD) and non-preferred direction (ND) with six levels of ambiguity per direction. Firstly, we estimated parameters of the three models by fitting those models' responses to the electrophysiological data, and checked the requirement of reasonableness, whether or not estimated parameters of each model satisfies functional and biological constraints. Next, we performed the leave-one-out cross-

1 Interdisciplinary Graduate School of Science and Engineering, Tokyo Institute of Technology, Yokohama, Kanagawa 226–8502, Japan
2 Department of Biology, University of Maryland, MD 20742, USA
3 School of Life Science, Tokyo University of Pharmacy and Life Sciences, Hachioji, Tokyo 192–0392, Japan
4 School of Computing, Tokyo Institute of Technology, Yokohama, Kanagawa 226–8502, Japan
a) ikeda.h.al@m.titech.ac.jp

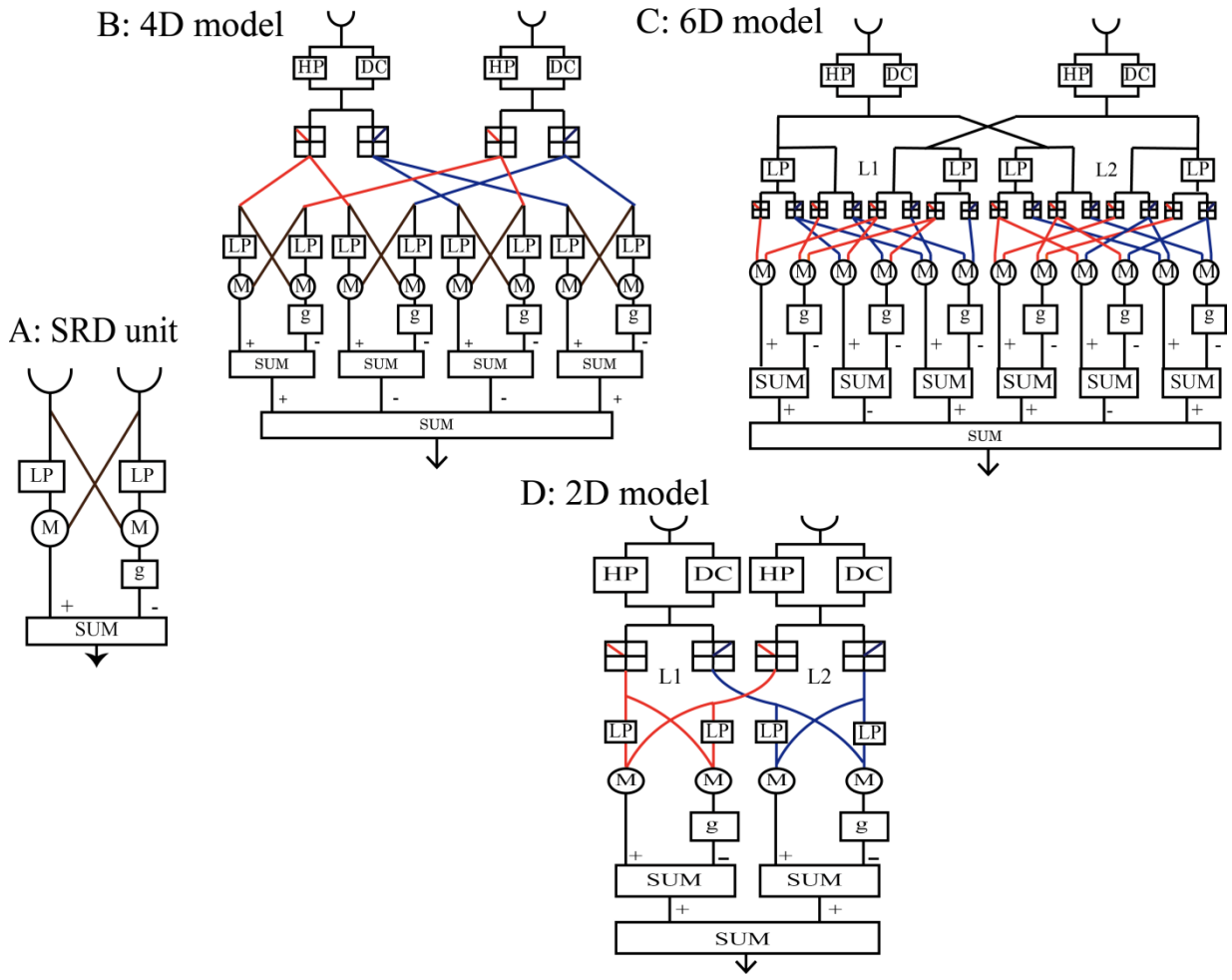

Fig. 1 Elementally motion detection (EMD) models we compare. A: Standard Reichardt detector (SRD) unit. The following three models compared here are composed of several number of SRD unit. B: 4D model consisting of four SRD units. C: 6D model consisting of six SRD units. D: 2D model consisting of two SRD units. HP is high-pass filter defined in Eq. (1), LP is low-pass filter defined in Eq. (2) and DC is direct connection to pass a signal directly. A relative synaptic weight, g, represents asymmetry between excitatory and inhibitory postsynaptic potentials ($0 \leq g \leq 1$). The three models in B, C and D have the common three parameters needed to be tuned individually: the time constants of the LP and HP, τ_l and τ_h, and the relative synaptic weight, g.

validation to evaluate the generalization error (GE) of the three models. Finally, we selected the most appropriate model in view of both the GE and reasonableness of estimated parameters in each of the three models. Through the model selection process, we concluded that the 2D model was most appropriate for explaining the data and satisfying functional and biological constraints. Furthermore, the result obtained here suggests coding properties in LPTCs.

2. Methods

2.1 Elementary Motion Detection Models

2.1.1 Common Structure of EMD Models

The 2D model in Fig. 1 D, the 4D model in Fig. 1 B and the 6D model in Fig. 1 C compared here are composed of several number of the standard Reichardt detector unit shown in Fig. 1 A. The SRD unit consists of two low-pass filters (LPs), two multipliers and one subtracter [1], [2], [12]. The SRD unit calculates cross-correlations of two opposite combinations of delayed and non-delayed signals of neighboring photoreceptors in a symmetrical fashion, and finally outputs a difference of the two time-lagged cross-correlations [12].

The LP commonly used here is a simple first-order lag system. The transfer function of the filter is

$$\mathrm{LP}(s) = \frac{1}{1 + \tau_l s}, \tag{1}$$

where τ_l is a time constant of the LP. The same LPs had been commonly used in the original 2D, 4D and 6D models [3], [6], [11], [13]. To align the conditions of the three models compared here, the three models use the same simple high pass filter (HP) and direct connection (DC) connected in parallel, which works as the band-stop filter. The same parallel filter had been used in the 2D model [3]. The transfer function of the HP is

$$\mathrm{HP}(s) = \frac{\tau_h s}{1 + \tau_h s}, \tag{2}$$

where τ_h is a time constant of the HP [3], [6], [11], [13]. The DC commonly used in the three models allows a signal to pass for all frequencies with attenuation to 10% of its original intensity for all frequencies [3]. We use the same value of attenuation as that of previous studies [3], [11].

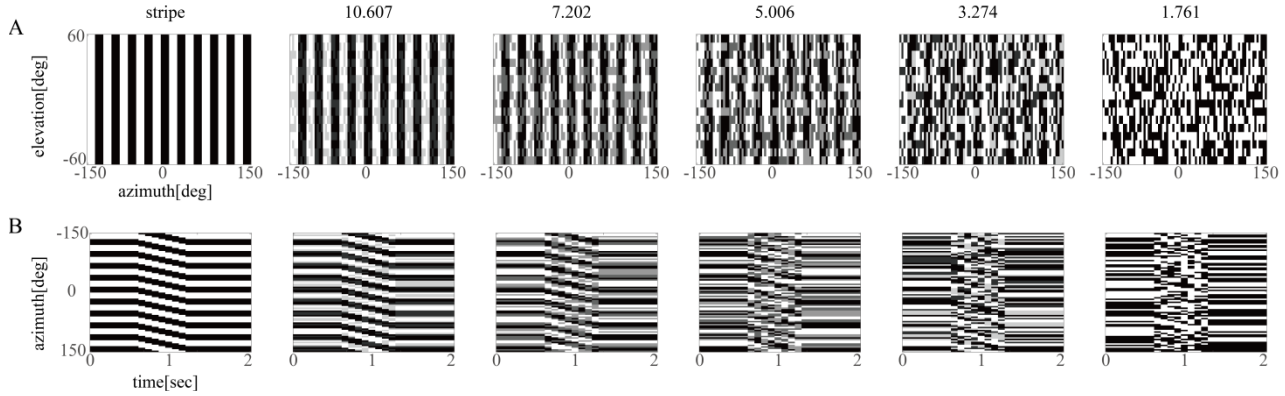

Fig. 2 Motion stimuli used in previous electrophysiological experiment [11] and in the following numerical simulations. The motion stimuli were panoramic vertically striped square-wave gratings with six different noise levels. The six panels in A and B show examples of stimuli of all different noise levels. A: Spatial plot of stripe stimuli (elevation [deg] vs azimuth [deg]). The SNR of each stimulus, which was defined in Eq. (3), is indicated at the head of each panel. B: Spatial-temporal plot of stripe stimuli (azimuth [deg] vs time [sec]). Each frame of stimuli was composed of 80×16 pixels that spanned 300 degrees in azimuth and ±60 degrees in elevation. The stripe width was 8 pixels. The stimuli were rotated clockwise and counterclockwise with frame rate of 8 Hz, the rotation speed was 30 degrees per second, and the duration of the rotation was 1 second. A total of 12 stimulation conditions consisting of PD and ND stimuli with the six noise levels per direction have been applied.

A relative synaptic weight g before the subtracter in the SRD unit is a relative synaptic weight that represents asymmetry between excitatory and inhibitory postsynaptic potentials ($0 \leq g \leq 1$) [13], [14], which had been commonly used in the original 2D, 4D and 6D models [3], [6].

In the implementation, these models are arranged in a two-dimensional 80×16 grid, and photoreceptors that are one to one paired to each element of these models are also arranged in a two-dimensional 80×16 grid (as in **Fig. 2** A, in Ref. [11]). The output of the models is defined as the sum of output from all the elements arranged in the 80×16 grid.

2.1.2 4D Model

Figure 1 B shows the 4D model that consists of four SRD units [3], [6].

Hassenstein et al. pointed out the issue on the difficulty of the biological implementation of the SRD unit because of the multiplication of negative and positive signals [3], [6], [7], and they remodeled the SRD unit to the 4D model that had been separated into the following four units receiving all possible four combinations of ON and OFF inputs: ON-ON, ON-OFF, OFF-ON and OFF-OFF SRD units under the rectification provided by four half-wave rectifies. Therefore, the 4D model used here is basically equivalent to the single SRD unit except for the existence of the HP and DC.

In performing estimation, we search the three parameters, the time constant of the LP, τ_l, the time constant of the HP, τ_h, and the relative synaptic weight, g.

2.1.3 6D Model

Figure 1 C shows the 6D model that consists of six SRD units [6], [9]. Clark et al. reported that both the L1 and L2 pathways can respond to ON-OFF and OFF-ON sequence stimuli, and they remodeled the 4D model to the 6D model that had been separated into two blocks representing the L1 and L2 pathways (Fig. 1 C). The block for the L1 pathway consists of ON-ON, ON-OFF and OFF-OFF SRD units, and the block for the L2 pathway consists of ON-ON, OFF-ON and OFF-OFF SRD units. The 6D model is basically equivalent to the 4D model and the single SRD unit even though there are two redundant components, but the position of half-wave rectifies in the 6D model is different from that of the 4D model (see Figs. 1 B and C). To align the conditions of the three models, we added the DCs in parallel with the HPs as being different from the original 6D model.

In performing estimation, we search the three parameters, the time constant of the LP, τ_l, the time constant of the HP, τ_h, and the relative synaptic weight, g.

2.1.4 2D Model

Figure 1 D shows the 2D model that consists of two SRD units [3], [15]. Eichner et al. reported that the L1 and L2 pathways could not respond to ON-OFF and OFF-ON sequence stimuli, whereas these could respond to ON-ON and OFF-OFF sequence stimuli. Following their experimental result, they modified the 4D model to the 2D model that consists of ON-ON and OFF-OFF SRD units (See Fig. 1 C). Thus, the response of the 2D model to visual stimuli is different from that of the 4D and 6D models. To align the conditions of the three models, we set a threshold of OFF-type half-wave rectifier to be 0 instead of 0.05 as being different from the original 2D model [3].

In performing estimation, we search the three parameters, the time constant of the LP, τ_l, the time constant of the HP, τ_h, and the relative synaptic weight, g.

2.2 Electrophysiological Data

Electrophysiological data reported in Suzuki et al. are used in the present work [11]. They recorded membrane potential of in-vivo horizontal system (HS) cells in the lobula plate of right hemisphere of *Drosophila melanogaster* using the whole-cell patch clamp technique. Its sampling frequency is 1 kHz. The whole data set consists of a total of 888 samples of membrane potential of seven HS cells (different individuals) in response to both preferred direction (PD) and non-preferred direction (ND) stimuli

with six noise levels per direction (a total of 12 stimulation conditions) as explained below. There are more than eight samples of membrane potential per individual per stimulation condition. Here, we averaged samples within each stimulation condition in each cell, and we obtained a total of 84 samples of membrane potential (corresponding to 12 conditions $\times$ 7 individuals). In the following numerical simulations, we sought to fit the model output to the averaged samples.

2.3 Motion Stimuli

Figure 2 shows motion stimuli used in electrophysiological experiments done by Suzuki et al. [11]. The motion stimuli used in Suzuki et al. are also used in the following numerical simulations that fit the three models to their data.

The LED arena, which was composed of 80×16 pixels and spanned 300 degrees in azimuth and ± 60 degrees in elevation, displayed panoramic vertically striped square-wave grating rotating clockwise and counterclockwise with frame rate of 8 Hz. The stripe width was 8 pixels, i.e., approximately 30 degrees. The rotation speed was 30 degrees per second, and the duration of rotation was 1 second. As shown in Fig. 2, the ambiguity of motion stimuli was varied with six different levels of noise. They generated stimulus noise and controlled its level using the following procedure. In each frame of motion stimuli, pixels of the LED arena were randomly selected with a probability of 0.4. They assigned a specific intensity of the random dot (RI) to the randomly selected pixels. If a pixel within those selected pixels was located on bright bars in the original stripe pattern, its intensity value became the subtraction of RI from the bright bar intensity. Note that the bright bar's intensity was 1.0. Otherwise, a pixel within those selected pixels was turned on with the value of RI. In the previous work, they used six levels of RI: 0, 0.2, 0.4, 0.6, 0.8 and 1.0. They introduced the following signal-noise ratio (SNR) to quantify the ambiguity of the motion stimuli,

$$\mathrm{SNR} = 10 \log_{10} \frac{1 - 0.4\mathrm{R_I}}{0.4\mathrm{R_I}}. \tag{3}$$

The SNRs of the six stimuli corresponding to the six levels of RI are indicated at the head of the panels in Fig. 2. They used a total of 12 stimulation conditions consisting of clockwise and counterclockwise rotation stimuli (i.e., PD and ND stimuli) with six noise levels per direction.

Following the above procedure, we also synthesized motion stimuli (80×16 pixels in each flame) with the same 12 conditions, and provided the synthesized stimuli to photoreceptors of these models arranged in the 80×16 grid.

2.4 Parameter Estimation and Model Selection

2.4.1 Mean Square Error between Data and Rescaled Model Outputs

To evaluate fitness between model output and membrane potentials of the HS-cell, we calculated the mean square error (MSE) between them for two seconds from the start of the rotation to 1 sec after the rotation stops.

Because the output of these models is dimensionless quantity, we need to adjust the scale of the model output to that of the membrane potential of the HS-cells. Firstly, we evaluated a scale factor for each HS-cell by calculating the ratio of two temporal averages of the model output and membrane potential of each HS-cell for the duration of rotation (i.e., one second) when using the PD stimulus in zero noise condition. Next, with respect to each HS-cell, all the model outputs in 12 stimulation conditions were rescaled with the scale factor estimated in zero noise condition, and we calculated the MSE between membrane potentials of each cell and the rescaled model outputs. Finally, we obtained the total MSE by averaging the MSE with respect to each HS-cell.

2.4.2 Grid Search

The three models compared here (Figs. 1 B, C and D) have the common three parameters needed to be tuned individually: the time constant of the LP in each SRD unit, τ_l, the time constant of the HP, τ_h and the relative synaptic weight, g. The parameter estimation was performed with grid-search over a parameter grid in the three-dimensional parameter space. The parameter grid consists of 20 grid points along the τ_h axes at equal intervals from 30 msec to 600 msec, 50 grid points along the τ_l axes at equal intervals from 20 msec to 1,000 msec and 21 grid points along the g axis at equal intervals from 0 to 1. Thus, we exposed 21,000 combinations of parameter values over the parameter grid to find the minimum point of the MSE.

2.4.3 Cross-validation for Model Selection

Model selection with the data of all seven individuals: The whole data obtained from seven individuals consists of 84 samples as explained above. We performed the leave-one-out cross-validation (LOOCV) to evaluate the generalization error (GE) of the three models. Of the 84 samples, a single sample was retained as the validation data for evaluating the models' GE quantified using the MSE, and the remaining 83 samples were used as training data for estimating the parameters of the models with the grid-search. Repeating the cross-validation process with each of the 84 samples used exactly once as the validation data, we obtained 84 MSEs quantifying the GE of each of the three models. The significance of the difference between the GEs of all possible pairs of the models was tested using the Wilcoxon signed rank-sum test.

3. Results

3.1 Parameter Estimation with Grid-search

The three models compared here (Figs. 1 B, C and D) have the common three parameters needed to be tuned individually: the time constants of the LP and HP, τ_l and τ_h and the relative synaptic weight, g. The parameter estimation was performed with the whole data of all the seven individuals (84 samples). **Figure 3** shows dependency of the MSE on the parameters in each of the three models. The MSE of the individual models becomes minimum at the point marked with the asterisk * shown in Fig. 3. The minimum points are at $\tau_\mathrm{h} = 360$ [msec], $\tau_\mathrm{l} = 260$ [msec] and g = 0.70 in the 2D model, at $\tau_\mathrm{h} = 120$ [msec], $\tau_\mathrm{l} = 400$ [msec] and g = 0 in the 4D model and at $\tau_\mathrm{h} = 120$ [msec], $\tau_\mathrm{l} = 400$ [msec] and g = 0 in the 6D model, respectively. In the 4D and 6D models, the estimates of the relative synaptic weight, g are equal to zero (Fig. 3 E and F).

Figure 4 shows results of numerical simulations with the best-fitting parameters in each of the three models in response to the

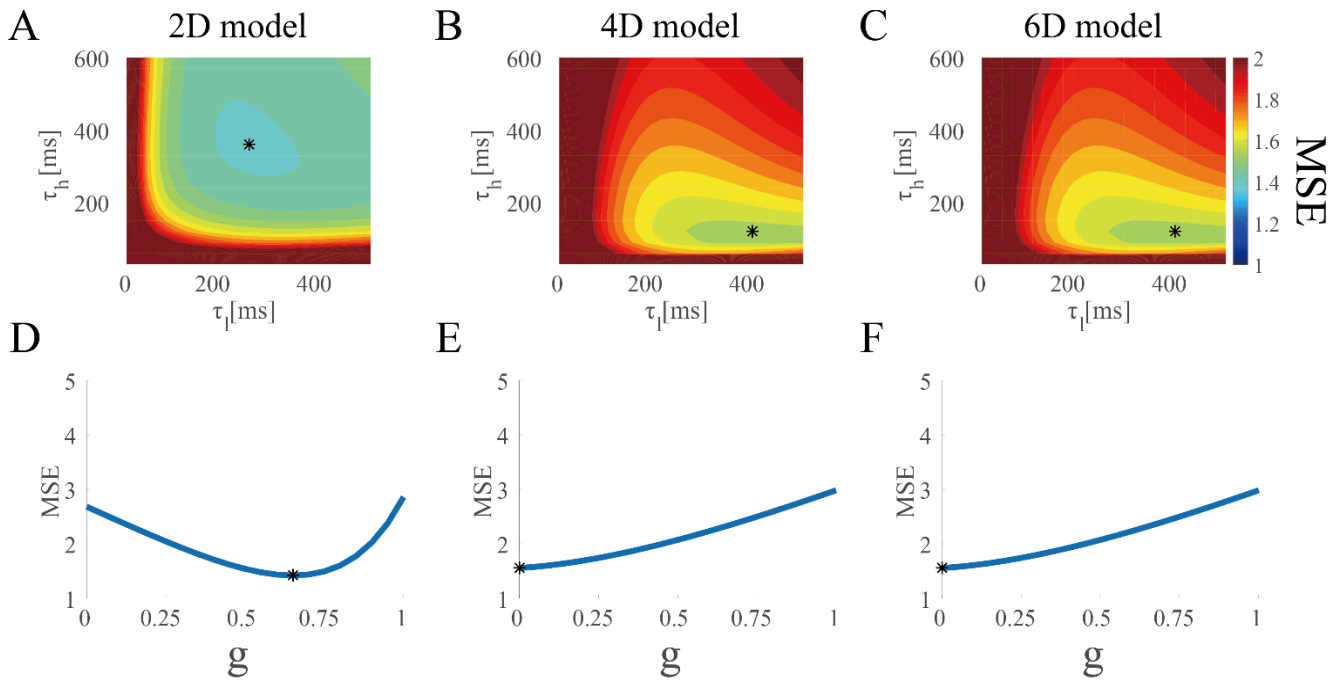

Fig. 3 Dependency of the MSE on the parameters in the three models when fitted to the data of all the seven individuals. A, B and C: The three panels show the dependency of the MSE on τ_l [msec] and τ_h [msec] in the 2D, 4D and 6D models, respectively. D, E and F: The three panels indicate the dependency of the MSE on g in the 2D, 4D and 6D models, respectively. Other parameters not plotted in each panel are set to be optimal. The MSE of the individual models becomes minimum at the point marked with the asterisk *.

12 different stimuli consisting of PD and ND stimuli with the six noise levels per direction. We superimposed examples of the membrane potential of the HS-cell most fitted to the results of numerical simulations on Fig. 4. Compared to the 2D model, responses of the 4D and 6D models to the ND stimuli are not in good agreement with the membrane potential responses of the HS-cell as shown in Fig. 4. This tendency is kept in almost all other samples.

3.2 Cross-validation for Model Selection and Variation among Individuals

We performed the LOOCV with the whole data obtained from seven individuals (84 samples), and we obtained 84 MSEs on the validation data, which quantify the GE, with 84 times validation process for each of the three models. **Figure 5** shows distributions of the 84 MSEs of the three models using scatter plots. We checked the significance of the difference between GEs of all possible pairs of the models. As shown in Fig. 5, the GE of the 2D model was significantly smaller than those of both the 4D and 6D models. Note that variation of the parameters estimated in each LOOCV iteration was 8.4% (the standard deviation divided by the mean) in the HP time constants of 4D model, which was largest in those of the parameters in the three models.

4. Discussions

4.1 Reasonability of the 2D Model

The results obtained from the LOOCV suggest that the final candidate is the 2D model.

As shown in Figs. 3 E and 3 F, the estimates of the relative synaptic weight, g were equal to zero. In principle, if g = 0, the 4D and 6D models, which are basically equivalent to the single SRD unit in Fig. 1 A, cannot respond to an edge moving in ND. **Figure 6** A shows a numerical example of non-negative (i.e., non-hyperpolarized [7]) response of the 6D model with g = 0 to the ND single edge stimulus. On the other hand, in the case of vertical stripe stimuli that are spatially and temporally periodic, the ON-OFF and OFF-ON SRD units can respond to the ND stimuli. We confirmed with numerical simulations that if g was equal to zero, hyperpolarized responses of the 4D and 6D models to the ND stimuli (lower row panels of Figs. 4 B and 4 C) were mainly induced by the ON-OFF and OFF-ON SRD units. Figure 6 B shows a schematic why the ON-OFF and OFF-ON SRD units can respond to the ND stripe stimuli. If τ_l is comparable to the temporal period of rotating stripes, the ON-OFF and OFF-ON SRD units can respond to such a periodic ND stimulus, because two successive bars in the stripe respectively provide OFF and ON sequence signals to the ON-OFF and OFF-ON SRD units, and cross-correlations of these OFF and ON sequence signals become compatible to the amplitude of PD responses due to the long delay by the LP. Therefore, the above speculations can give the following conclusion that the 4D and 6D models with the best-fitting parameters are not in functionally and biologically reasonable situations.

Finally, due to the result of LOOCV and non-reasonability of the 4D and 6D models fitted to the electrophysiological data, we can select the 2D model.

4.2 Verification and Comparison of the Three Models in Previous Works

As explained above, two different research groups respectively

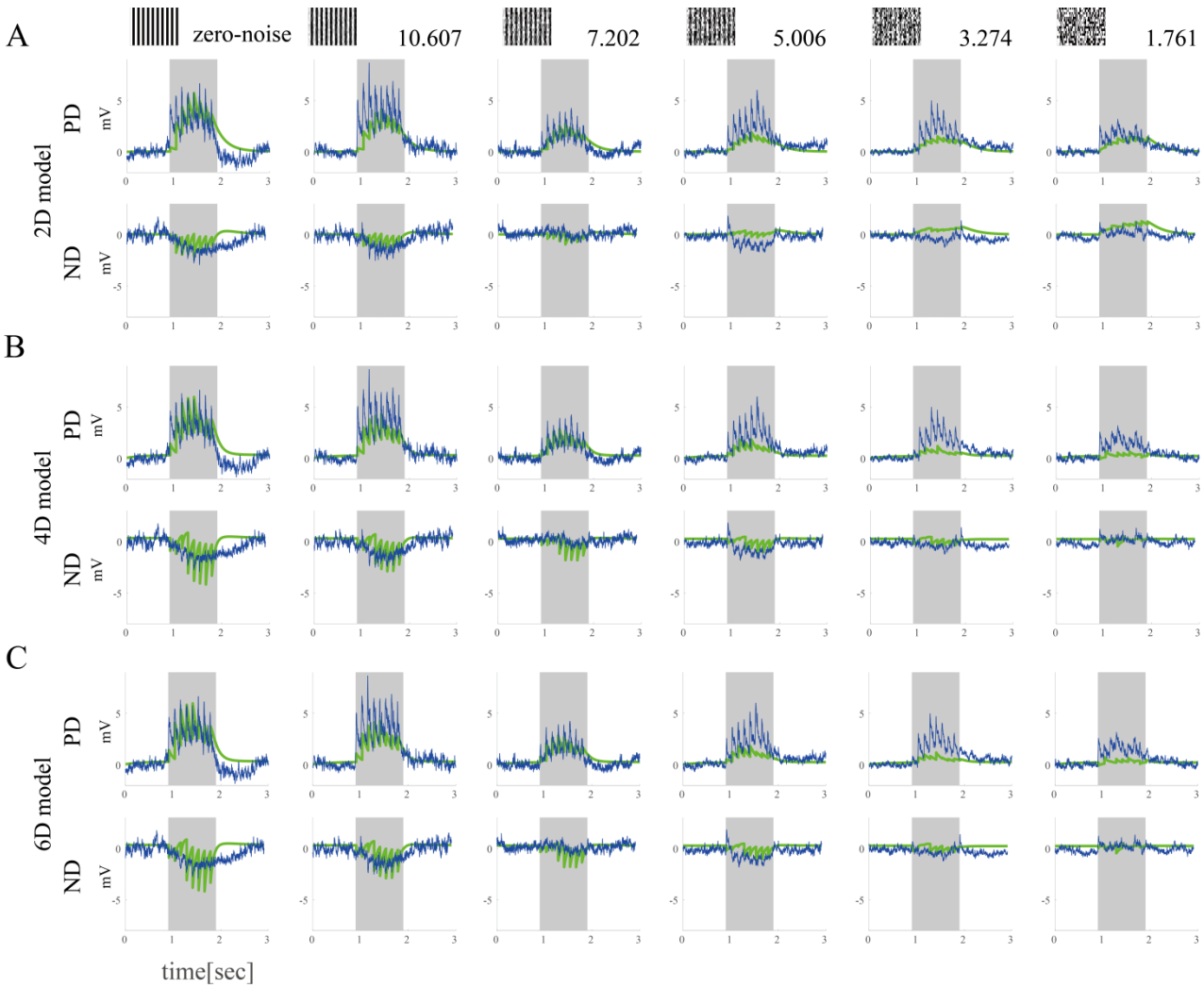

Fig. 4 Results of numerical simulations with the best-fitting parameters in each of the three models with the data of all seven individuals and examples of the membrane potential of the HS-cell in response to stimuli of 12 different conditions. A: 2D model. B: 4D model. C: 6D model. Green lines: simulation results of the each model. Blue lines: traces of the membrane potential of the HS-cell most fitted to the simulation results. Upper and lower row panels in A, B and C show the responses to PD and ND stimuli, respectively. The noise level of each stimulus is indicated at the top of this figure. Shaded region of each panel indicates the duration of rotation.

modified the 4D model to the 2D and 6D models to explain the responsiveness of the L1 and L2 pathways. The reasonability and parameters of each of the 2D and 6D models have been verified on the basis of the following different experiment. Eichner et al. verified the reasonability of 2D model and manually tuned its parameters on data of membrane potentials traces of VS cells in response to apparent motion step stimuli in the four different stimulus conditions consisting of four combinations of ON and OFF stripes appearing in sequence [3]. Clark et al. verified the structure of the 6D model on data acquired by calcium imaging targeted to the L1 and L2 pathways, and estimated its model parameters by measuring behavioral response to white noise visual stimuli, i.e., by employing white noise analysis [6]. Joesch et al. have qualitatively compared the 2D and 6D models using membrane potential traces of VS cells in response to ON-OFF and OFF-ON sequence stimuli when each of L1 and L2 pathways had been blockade [9]. Leonhardt et al. have tuned the 2D model to maximize its motion detection ability to natural images, and claimed that parameters of the 2D model they tuned were qualitatively consistent with their electrophysiological data of LPTC [16].

However, there has not been a quantitative comparison of the 2D and 6D models. In this paper, we have firstly selected the most statistically appropriate model from the two models and the 4D model using the common experimental data.

4.3 Reasonableness of Estimates

As described in Section 4.2, the parameters of each of the 2D and 6D models had been estimated using the different experimental data set in the previous works [3], [6], [16]. Thus, for instance, the estimate of LP time constant was different from each other. Eichner et al. estimated the LP time constant of the 2D model as 50 msec using membrane potentials traces of VS cells, whereas Clark et al. estimated the LP time constant of the 6D model to be 10,000 msec using behavioral response data. Furthermore, Behnia et al. have reported that Mi1, Tm1, Tm2 and Tm3 cells in the medulla might function as the LP in the SRD unit, and the time constant mediated by these cells could be 13∼18 msec [17]. Leonhardt et al. have estimated the LP time constant of 2D model

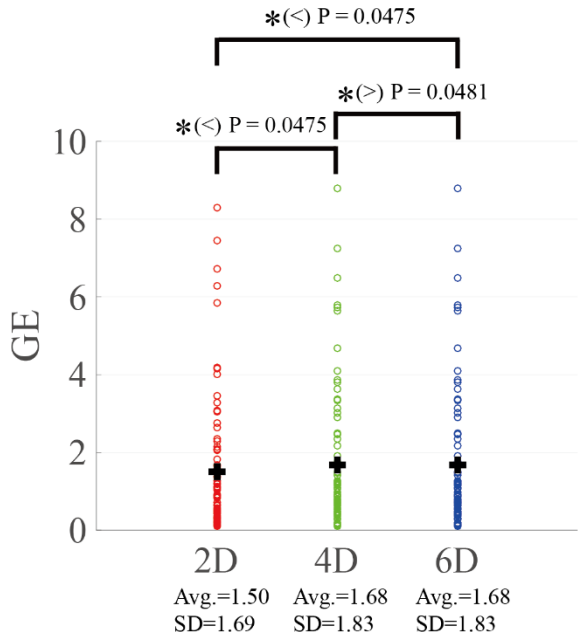

Fig. 5 Scatter plot of GEs quantified by the MSEs on the validation data. We performed the LOOCV with the whole data obtained from seven individuals (84 samples), and we plotted a distribution of MSEs obtained by 84 times validation process in each of the three models. A plus sign indicates the average point of the GE of the individual models. The standard deviations of the GEs are indicated at the bottom of the figure. The significance of the difference between GEs of all possible pairs of the models was tested using the Wilcoxon signed rank-sum test.

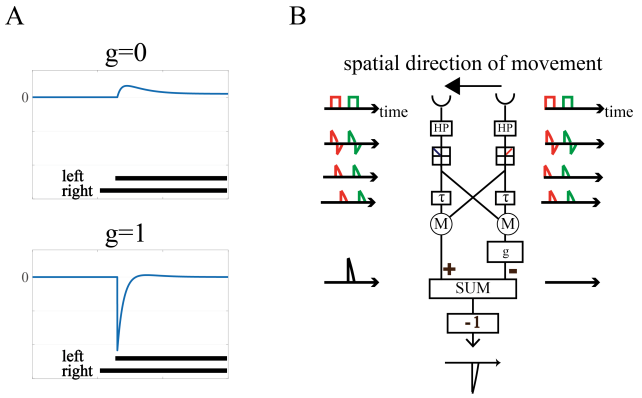

Fig. 6 Non-reasonability of the 6D model when g = 0. A: Non-negative response of the 6D model with g = 0 to a single bar stimulus rotating in ND. B: Schematic of mechanism why the ON-OFF and OFF-ON pathways are responsible to the ND stripe stimuli when g = 0. Two successive bars in the stripe respectively provide OFF and ON signals to this pathway, and cross-correlations of these OFF and ON signals become compatible to the amplitude of PD responses due to the LP with large τ_1.

to be 20∼120 msec by a comparison of the electrophysiological data of LPTC and the 2D model optimally tuned to natural images [16].

On the other hand, we estimated the LP time constant of the 2D model to be 260 msec and those of the 4D and 6D models to be 400 msec. Thus, our estimate of the LP time constant in the 2D model was larger than those of Eichner et al. and Borst et al., and our estimate in the 6D model is smaller than that of Clark et al. The reasons of the difficulty we speculate are that the stimuli we used in measuring membrane potential responses was different from those of the previous works as described above, and we used the membrane potential traces whereas Clark et al. used the behavioral data. Our estimation was performed using the data acquired in more various stimulation conditions than those of the previous works, and thus we could reduce the possibility of over-fitting in parameter estimation compared to the previous work.

4.4 Whether L1 and L2 Pathways could Respond to ON-OFF and OFF-ON Stimuli or Not?

As explained above, our quantitative comparison of the three models has strongly suggested that the 2D model might be suitable for explaining the data of membrane potential traces of HS cells. Eichner et al. used the 2D model, which only consists of ON-ON and OFF-OFF units, to explain their hypothesis based on the experimental data that the L1 and L2 pathways could not respond to ON-OFF and OFF-ON sequence stimuli. Our result obtained from the quantitative comparison also gave a possibility that the L1 and L2 pathways could not respond to ON-OFF and OFF-ON sequence stimuli, and thus support the Eichner's hypothesis. However, it is impossible to determine the function of each of the L1 and L2 pathways through the quantitative comparison performed here. This is because we could not separate a single membrane potential trace into two signals delivered from the L1 and L2 pathways individually, and could not uniquely identify the response characteristic of each of the L1 and L2 pathways from the single potential trace. To overcome this issue, we have to verify extra data acquired from either L1 or L2 pathway blockade fly as in the previous works [16], [18].

5. Conclusion

As described in Section 4.1, due to the result of LOOCV and non-reasonability of the 4D and 6D models fitted to the electrophysiological data, we can select the 2D model.

References

[1] Borst, A., Haag, J. and Reiff, D.F.: Fry Motion Vision, *Annual Review of Neuroscience*, Vol.33, pp.49–70 (2010).
[2] Borst, A.: Fly visual course control: Behaviour, algorithms and circuits, *Nature Reviews Neuroscience*, Vol.15, pp.590–599 (2014).
[3] Eichner, H., Joesch, M., Schnell, B. et al.: Internal Structure of the Fly Elementary Motion Detector, *Neuron*, Vol.70, Issue 6, pp.1155–1164 (2011).
[4] Sanes, J.R. and Zipursky, S.L.: Design Principles of Insect and Vertebrate Visual Systems, *Neuron*, Vol.66, Issue 1, pp.15–36 (2010).
[5] Borst, A. and Helmstaedter, M.: Common circuit design in fly and mammalian motion vision, *Nature Neuroscience*, Vol.18, pp.1067–1076 (2015).
[6] Clark, D.A., Bursztyn, L., Horowitz, M.A., et al.: Defining the Computational Structure of the Motion Detector in *Drosophila*, *Neuron*, Vol.70, Issue 6, pp.1165–1177 (2011).
[7] Borst, A.: In search of the Holy Grail of fly motion vision, *European Journal of Neuroscience*, Vol.40, pp.3285–3293 (2014).
[8] Gabbiani, F. and Jones, P.W.: A Genetic Push to Understand Motion Detection, *Neuron*, Vol.70, Issue 6, pp.1023–1025 (2011).
[9] Joesch, M., Weber, F., Eichner, H. and Borst A.: Functional Specialization of Parallel Motion Detection Circuits in the fly, *The Journal of Neuroscience*, Vol.33, No.3, pp.902–905 (2013).
[10] Borst, A.: Correlation versus gradient type motion detectors: the pros and cons, *Philosophical Transactions of the Royal Society B*, Vol.362, Issue 1479, pp.369–374 (2007).
[11] Suzuki, Y., Ikeda, H., Miyamoto, T. et al.: Noise-robust recognition of wide-field motion direction and the underlying neural mechanisms in *Drosophila melanogaster*, *Scientific Reports*, Vol.5, No.10253 (2015).
[12] Hassenstein, B.: A Cross Correlation Process in the Nervous Center of

an Insect Eye, *Nuovo Cimento*, Vol.13, Series 10, Supplement (1959).
[13] Egelhaaf, M. and Borst, A.: Are there separate ON and OFF channels in fly motion vision?, *Visual Neuroscience*, Vol.8, Issue 2, pp.151–164 (1992).
[14] Egelhaaf, M. and Borst, A.: Computational structure of a biological motion-detection system as revealed by local detector analysis in the fly's nervous system, *Journal of Optical Society of America*, Vol.6, No.7, pp.1070–1087 (1989).
[15] Stavenga, D.G. and Hardie, R.C. (Eds.): Facets of Vision, softcover reprint of the hardcover 1st edition, Franceschini, N., Riehle, A. and Le Nestour, A.: *Directionally Selective Motion Detection by Insect Neurons*, pp.360–390, Springer-Verlag, Berlin Heidelberg (1989).
[16] Leonhardt, A., Ammer, G., Meier, M., et al.: Asymmetry of *Drosophila* ON and OFF motion detectors enhances real-world velocity estimation, *Nature Neuroscience*, Vol.19, pp.706–715 (2016).
[17] Behnia, R., Clark, D.A., Carter, A.G. and Clandinin, T.R.: Processing properties of ON and OFF pathways for *Drosophila* motion detection, *Nature*, Vol.512, pp.427–430 (2014).
[18] Brand, A.H. and Perrimon, N.: Targeted gene expression as a means of altering cell fates and generating, *Development*, Vol.118, pp.401–415 (1993).

Hideaki Ikeda received his B.E. degree from Nihon University in 2013, and his M.S. degree from Tokyo Institute of Technology. He is currently a doctoral student at Interdisciplinary Graduate School of Science and Engineering, Tokyo Institute of Technology.

Yoshinori Suzuki received his Ph.D. degree from Tokyo institute of Technology in 2015. He is currently a postdoctoral researcher at University of Maryland.

Takako Morimoto received her Ph.D. degree from Osaka University in 1992. She is currently an associate professor at School of Life Science, Tokyo University of Pharmacy and Life Sciences.

Toru Aonishi received his B.E. degree from Kyusyu Institute of Technology in 1993, and his M.E. and D.E. degrees from Osaka University in 1995 and 1998, respectively. He was a researcher at RIKEN Brain Science Institute from 1998 to 2004. He is currently an associate professor at School of Computing, Tokyo Institute of Technology. His research focuses on non-linear dynamics, statistical mechanics and theoretical neuroscience.